Pergamon

Cement and Concrete Research, Vol. 26, No. 5, pp. 729-741, 1996

0008-8846/96 $15.00 + .00

PII S0008-8846(96)00051-8

STABILITY OF FRIEDEL'S SALT IN CARBONATED CONCRETE STRUCTURAL ELEMENTS

A.K. Suryavanshi, and R. Narayan Swamy
Department of Mechanical and Process Engineering, University of Sheffield, Sheffield, S1 2DU, UK

(Refereed)
(Received August 15, 1995; in final form March 12, 1996)

ABSTRACT

It is of significant scientific and engineering benefit from the corrosion view point, to know the state of Friedel's salt in concrete structures subjected to the simultaneous attack of chlorides and atmospheric carbonation. An attempt is made in the present experimental investigation to elucidate the role of atmospheric carbonation on the stability of the Friedel's salt in chloride contaminated structures. For this purpose, four different types of concrete slabs, were subjected to chloride penetration over a total period of about three years and then exposed to atmospheric carbonation for almost the same period. The stability of Friedel's salt, based on XRD and DTA results is shown to be pH dependant. The solubility of Friedel's salt increases with the degree of carbonation of the concrete. It is also concluded that the stability of ettringite is also pH dependant.

Introduction

There are several ways by which chloride ions in concrete bind with the cement hydration products. The chloride ions bind in the form of a tri-chloro-complex, $3CaO.3CaCl_2.Al_2O_3.10H_2O$.aqueous, at -10°C by the hydration of tri-calcium aluminate (C_3A) in 23% $CaCl_2$ solution (1). The chlorides also bind in the form of a complex compound containing $CaCl_2$, $Ca(OH)_2$, and/or $CaCO_3$ below 20°C when $CaCl_2$ concentration in the solution is higher than 15% (2). Under field conditions, however, both the above chloro-complexes do not generally form. Apart from the above two chemical interactions, the possibility of interaction of $CaCl_2$ with the C-S-H gel has been reported (3–6). This has been disputed by Lambert et al who however, used NaCl (7). Considerable evidence from laboratory investigations and field structures, however, suggest that, the C_3A and tetra-calcium aluminoferrite (C_4AF) phases of the cement are responsible for the binding of chloride ions to form "Friedel's salt," $3CaO.Al_2O_3.CaCl_2.10H_2O$, and its ferrite analogue, $3CaO.Fe_2O_3.CaCl_2.10H_2O$ respectively (8–12).

The disassociation of the bound chlorides in the form of Friedel's salt, during the service life of the concrete structure, subjects the steel to a greater corrosion risk. This is because, out of the total chlorides (free chlorides + bound chlorides) only the free-chlorides are responsible for

depassivating the reinforcement steel. This emphasises the need for the Friedel's salt to remain stable during the service life of a concrete structure contaminated with chlorides. No direct scientific evidence in the published literature so far suggests the breakdown of Friedel's salt in chloride contaminated concrete during its service life. However, investigation carried out by Page and Vennesland (13) with cements blended with silica fume suggests indirectly the possibility of increased solubility of Friedel's salt. In their study, substantial changes in pore solution alkalinity and chloride binding were observed with 10%, 20% and 30% cement replacements by silica fume. For example, with 30% cement replacement by silica fume and 1% Cl^- addition by weight of binder, the pH of the pore solution dropped by three orders of magnitude from ~pH 14 (100% cement) to ~pH 11. Also, the capacity of the cement to bind chloride ions introduced during mixing decreased disproportionately with the cement replacement. This lead the authors to conclude that, the significant decrease in pore solution alkalinity in the presence of silica fume increased the solubility of Friedel's salt to release the bound chlorides into the pore solution. Thus, the stability of Friedel's salt in concrete appears to be pH dependant. Applying the same analogy, Friedel's salt present in chloride contaminated concrete structures should also breakdown in the event of carbonation of concrete, which can lower the concrete alkalinity to as low value as about pH 8.5 (14).

In the present investigation, an attempt is made to elucidate the stability of the Friedel's salt formed in concrete slabs which were subjected to both chloride ingress and atmospheric carbonation.

Experimental Work

To investigate the long term diffusion characteristics of chlorides through concrete, various reinforced concrete slabs were cast having different water-binder (w/b) ratios incorporating a variety of mineral admixtures such as silica fume (SF), ground granulated blast furnace slag (GGBFS) and fly ash (FA), and surface treatments (surface coating and textile membrane). Four of these were selected for the present investigation. The details of these four slabs are given in Table 1. The w/b ratio for slabs 3 and 10 was 0.75 while, for the slab 11 it was 0.6. Slab 1 was used for comparison purpose as it represents an ideal concrete with a low w/b ratio of 0.45, which is unlikely to allow large penetration of chlorides. Ordinary portland cement (OPC) containing 9% C_3A and 7% C_4AF by weight was used for all the slabs.

Slab 11 was cast with a textile membrane at the bottom surface of the mould. The mould had pre-drilled holes to provide a path for the bleeding water to leak through the membrane after casting. The textile membrane is believed to create a homogeneous surface with minimum surface defects.

TABLE 1

The Details of the Slabs Used in the Investigation

Slab No	w/b ratio	Size in mm	Special features
1	0.45	1000X1000X150	50% surface coated with an acrylic rubber coating
3	0.75	1000X1000X150	As above
10	0.75	1000X500X150	65% cement replacement by weight with GGBFS
11	0.60	500X500X150	Textile membrane at the bottom of the mould

All the slabs had steel reinforcement of 20 mm diameter provided at an effective depth of 125 mm. At the time of casting, the slabs were provided with an acrylic frame of 50 mm height; this frame formed an embankment on the top surface of the slabs for ponding of the salt solution. For slab 11 ponding was done at the top cast surface which was not in contact with the textile membrane. After curing for 28 days, all the slabs were exposed to a series of chloride penetration regime consisting of 7 days of ponding with 4% sodium chloride solution followed by 3 days of drying. Freshly prepared sodium chloride solutions were used for each ponding. All the slabs were subjected to a total of 70 cycles in steps of 10, 20, 50, and 70 cycles. Short time gaps (few days) were maintained between 10 and 20, 20 and 50 cycles. Longer time gap of about one and half year existed between 50 and 70 cycles. After the completion of 70 cycles of ponding and drying, the slabs were left exposed to a laboratory drying environment for about two and half years similar to that of an interior of a building. All the slabs are now nearly six years old.

The first stage of the experimental work consisted of establishing chloride profiles over the depths of the slabs. This was followed by the X-ray diffraction (XRD) and differential thermal analyses (DTA) of the hydrated cement powders to identify the chemical phases present. For this, the slabs were cored with a water lubricated vacuum based Hilti core cutter. Slab 11 was cored at four randomly selected locations to a depth varying between 105 mm and 115 mm. Slabs 1, 3 and 10 were also cored at six randomly selected locations (on the uncoated surface for slabs 1 and 3) to the same depth as above. The cores were then sliced using a water lubricated circular saw into the following depths: 0–5, 5–25, 25–45, 45–65, 65–85 and 85–105 mm. The sliced samples were then passed twice through a jaw crusher. To get a representative sample for each slab at a given depth, the sliced samples from the same depth were mixed. To separate the large aggregates, the coarsely crushed samples were then passed through a 2 mm sieve. The coarsely crushed particles were finally crushed to a fine size by crushing them in a heavy duty pestle mortar. The crushed samples from the pestle mortar were then passed through a 150 μm sieve and the powder was used for chloride analyses and also for XRD and DTA studies.

The acid soluble chloride contents by weight of total cementitious contents were determined indirectly by Volhard's method as described in BS 1881 (15).

The powder method of X-ray diffraction was adopted in the present investigation. For this, a Phillips diffractometer with a X-ray source of Cu Kα radiation (λ=1.5418 Å) was used. The scan speed was 2° per minute and the scan-step was 0.02°. The X-ray tube voltage and current were fixed at 50 KV and 30 mA respectively.

A Stanton Redcroft DTA (model 673-4) was used for the thermal studies in the present investigation. Powdered samples weighing 100 mg were used to make the samples more representative, although this might result in thermal gradients within the sample. The samples were scanned from room temperature to 850°C. The scan speed was 10°C per minute. Powdered alumina was used as reference material. Platinum crucibles were used for filling both the reference material and the powdered sample.

Results

The results presented in the following sections are for the four slabs, that is, slab 1, 3, 10 and 11, after undergoing 70 cycles of 7 days of ponding and 3 days of drying with 4% sodium chloride solution, and subsequent exposure to a drying laboratory environment for about two and half years.

Chloride Analyses. Figure 1 presents the chloride profiles for all the four slabs as a function of depth from the surface of the slab. The data represented in Figure 1 shows the chloride profiles at the centre of the depths analysed that is, 45–65 mm depth interval for example, is represented by 55 mm depth. In general, all the slabs showed consistently decreasing chloride contents with increasing distances from the surface. For slabs 3 and 11, large quantities of chlorides were present even at substantial depths from the surface. However, for slabs 1 (w/b = 0.45) and 10 (w/b = 0.75, slab with slag) the chloride contents were almost nil beyond the 45–65 mm depth interval. Thus, Friedel's salt could be expected wherever the acid soluble chlorides are present, this will be verified by XRD. Comparison of the chloride profiles of slabs 1 (w/b = 0.45) and 3 (w/b = 0.75) signifies the importance of w/b ratio. The comparison of the chloride profiles of slabs 3 (w/b = 0.75) and 11 (w/b = 0.6) points to the apparent failure of the textile membrane in controlling the penetration of the chloride ions; instead it seems to have aggravated the penetration rate of chlorides beyond 75 mm depth from the surface.

The acid soluble chloride contents for the 0–5 mm depth interval were not analysed as abnormally high build-up of chlorides is expected at this depth of the slab. Build-up of large quantities of chlorides at this particular depth is because of its close proximity to the surface, and there is also the possibility of salt precipitation at this level during the drying period in the 10 days cycle. The presence of large quantities of chlorides near the surface of all the slabs is of great interest to the present investigation as carbonation is also expected in this area.

X-ray Diffraction and Dta Analyses. All the XRD diffractograms and the DTA thermograms presented in the following section are plotted with identical scale for the y-axis.

Slab 11. Figure 2 presents the X-ray diffractograms for 0–5 mm and 45–65 mm depth intervals. The diffractogram for the 0–5 mm depth interval shows strong maximum intensity (100%) peaks for α-quartz (SiO_2, hexagonal) at 3.34 Å and for calcite ($CaCO_3$, hexagonal) at 3.04 Å. The meta-stable calcium carbonates such as aragonite ($CaCO_3$, orthorhombic) and vaterite ($CaCO_3$, hexagonal) are also evident with their maximum intensity peaks at 3.40 Å and 2.09 Å respectively. The important observation, however, is the absence of portlandite ($Ca(OH)_2$), ettringite ($3CaO.3CaSO_4.Al_2O_3.32H_2O$), and Friedel's salt, although it is natural to expect

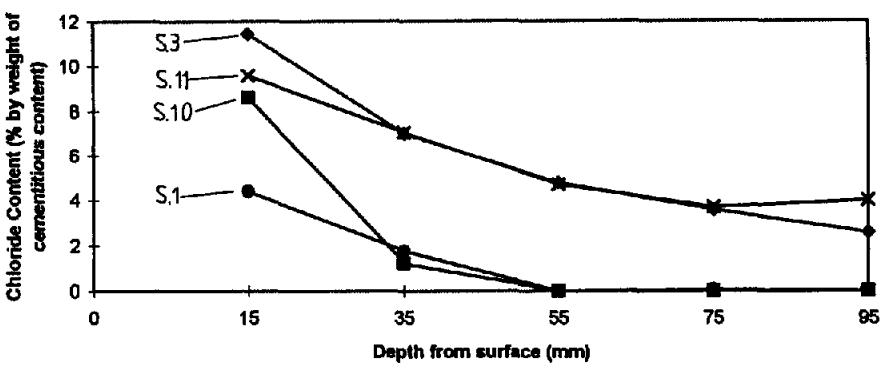

FIG. 1.
Acid soluble chloride profiles for slabs 1, 3, 10 and 11.

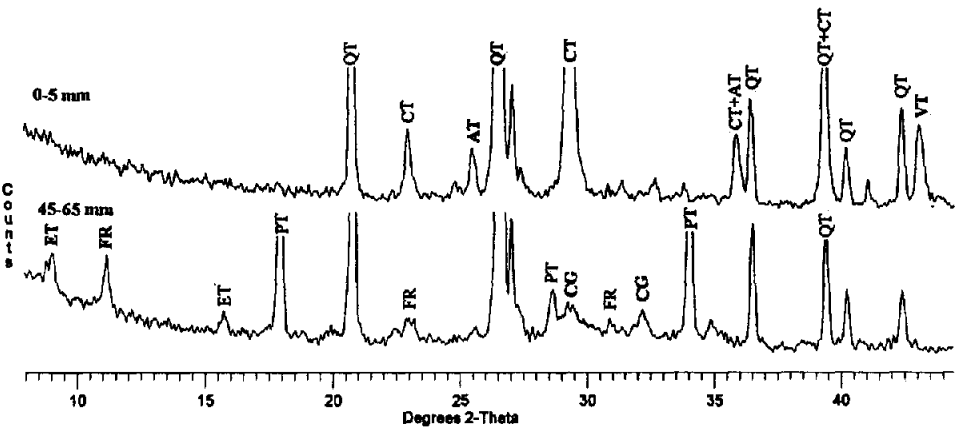

FIG. 2.
XRD diffractogram for slab 11. (Key: ET: Ettringite, FR: Friedel's salt, PT: Portlandite, QT: α-Quartz, AT: Aragonite, CT: Calcite, CG: C-S-H gel and VT: Vaterite. The keys in bold letters indicate the 100% intensity peaks).

Friedel's salt at this depth interval due to the presence of large quantities of acid soluble chlorides. The absence of portlandite is explained by its chemical reaction with the atmospheric CO_2 in the presence of moisture to form calcium carbonate (calcite, aragonite and vaterite). The α-quartz is believed to be from the sand used in producing the concrete and its presence is noticed in all the diffractograms presented here.

Contrary to the above, the diffractogram for the 45–65 mm depth interval shows the maximum intensity peaks for the Friedel's salt (monoclinic) at 7.9 Å, for portlandite (hexagonal) at 2.63 Å and ettringite (hexagonal) at 9.73 Å. However, the maximum intensity peak for $CaCO_3$ (calcite, aragonite and vaterite) is not evident, which implies the absence of severe atmospheric carbonation. The absence of $CaCO_3$ is indirectly supported by the presence of portlandite. A small peak appearing in the region of the maximum intensity peak for calcite is believed to be the poorly crystalline C-S-H gel as atmospheric carbonation is not expected at such substantial depths.

It is important to note that both Friedel's salt and its ferrite analogue, $3CaO.Fe_2O_3.CaCl_2.10H_2O$, appear at similar d-spacing in XRD diffractograms as they are iso-structural phases (11). However under comparable conditions, because of the higher reactivity of C_3A than the C_4AF, this results in the preferential crystallisation of Friedel's salt.

Incidentally, similar to Friedel's salt, tetra-calcium aluminate 13-hydrate, C_4AH_{13}, a meta-stable hydrate of C_3A, also has its maximum intensity peak at 7.9 Å (16). This makes the identification of Friedel's salt inconclusive by XRD alone. DTA is widely used for making a distinction between the Friedel's salt and C_4AH_{13} (5,8,9). The presence of Friedel's salt is indicated by an endothermic peak centered anywhere between 300°C to 350°C (5,8,9,11,17), with most reports suggesting the thermal event to be at or close to 350°C. The endothermic peak is due to the loss of crystalline water from the Friedel's salt (17). The different types of instrumentation used may be one of the reasons for the large variations in the reported temperatures. The presence of C_4AH_{13} results in a series of endothermic peaks below 300°C

at 280°C, 190°C, 125°C, 90°C and at 75°C (18). These endothermic responses indicate the gradual loss of crystalline water from the C_4AH_{13} phase with increasing temperature. The presence of calcite with its maximum intensity peak at 3.04 Å is also inconclusive from the XRD results alone as the C-S-H gel also has its maximum intensity peak at 3.07 Å (16). The presence of calcite can also be confirmed on DTA thermogram by an endothermic peak centered around 800°C due to its decomposition into calcium oxide, CaO (19). However, in normally hydrated portland cements, the C-S-H gel is known to be nearly amorphous and hence is not expected to give a dominant response on XRD diffractograms.

Similarly the presence of ettringite, portlandite and α-quartz can also be confirmed on DTA thermograms. The presence of ettringite manifests through an endothermic peak centered around 140°C due to the loss of crystalline water (20). The portlandite dehydrates to CaO at about 400°C; on DTA thermogram, it therefore gives rise to a strong peak around 500°C (21). The presence of α-quartz can be confirmed by an endothermic peak at 573°C at which it transforms into β-quartz (16).

Figure 3 depicts the DTA thermograms for 0–5 mm and 45–65 mm depth intervals. The thermogram for the 0–5 mm depth interval does not indicate the presence of Friedel's salt through an endothermic peak in the expected temperature range. In addition, both portlandite and ettringite are also not seen at the expected temperatures. On the other hand, a large endothermic peak centered at 790°C confirms the presence of calcite.

Alternatively, the DTA thermogram for the 45–65 mm depth interval illustrates a definite endothermic peak centered at 345°C for the Friedel's salt, which is within the expected temperature range. Apart from the Friedel's salt, the thermogram also shows a well defined endothermic peak for portlandite centered at 485°C. There is no endothermic peak centered around 800°C to suggest the presence of calcite. The thermogram also indicates the presence of ettringite through a weakly defined endothermic peak centered at 145°C. Thus, the DTA results confirm all the XRD findings for both the depth intervals.

The dominant endothermic peak centered around 120°C in all the thermograms presented here is due to the loss of free-water from the powdered sample. Similarly, all the thermograms show the presence of α-quartz through an endothermic peak centered around 570°C.

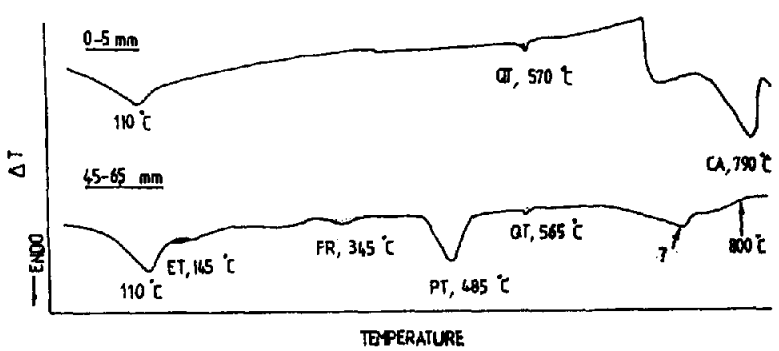

FIG. 3.
DTA thermograms for slab 11. (Key: ET: Ettringite, FR: Friedel's salt, PT: Portlandite, QT: α-Quartz, CA: Calcite).

From the above results, it is quite evident that both Friedel's salt and ettringite do not exist when $CaCO_3$ is present in dominant proportions as calcite, vaterite and aragonite, and the presence of $CaCO_3$ in dominant proportions is supported by the absence of portlandite.

Slab 3. Figure 4 shows the XRD diffractograms for 0–5 mm and 5–25 mm depth intervals. The XRD diffractogram for the 0–5 mm depth interval is similar to that of the 0–5 mm depth interval for slab 11 in some respects, and indicates the maximum intensity peaks for calcite, aragonite and vaterite. However, contrary to slab 11, small maximum intensity peaks for Friedel's salt, portlandite and ettringite are seen.

On the other hand, in the diffractogram for the 5–25 mm depth interval, the maximum intensity peaks for both Friedel's salt and portlandite grew in intensities in the presence of a small maximum intensity peak for calcite.

The relatively small peak for calcite may suggest the diminution in the quantity of calcite compared to that in the diffractogram for the 0–5 mm depth interval. The XRD indicates the presence of ettringite.

Figure 5 presents the thermograms for 0–5 mm and 5–25 mm depth intervals. In the thermogram for the 0–5 mm depth interval, the endothermic peak centered at 355°C for the Friedel's salt is not clearly defined. Alternatively, it is clear and definite (centered at 360°C) in the thermogram for the 5–25 mm depth interval. Similarly, in conformity with XRD results, the endothermic peak centered at 785°C for calcite, which was relatively small for the 5–25 mm depth interval is dominant (at 810°C) in the thermogram for the 0–5 mm depth interval. Carbonation to some extent at 5–25 mm depth interval is understandable because of the higher w/b ratio (0.75).

The presence of a small quantity of portlandite as seen from XRD results is not evident in the thermogram for the 0–5 mm depth interval. This might be due to the thermal event related to the portlandite falling below the sensitivity of the instrument. However, the endothermic peak for portlandite centered at 495°C is clear and dominant in the thermogram for the 5–25 mm depth interval confirming the findings from XRD.

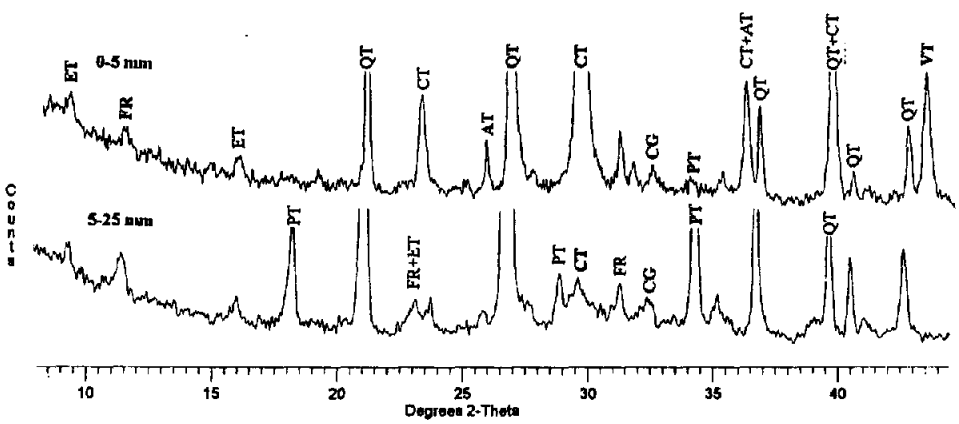

FIG. 4.

XRD diffractograms for slab 3. (Key: ET: Ettringite, FR: Friedel's salt, PT: Portlandite, QT: α-Quartz, AT: Aragonite, CT: Calcite, CG: C-S-H gel and VT: Vaterite. The keys in bold letters indicates the 100% intensity peaks).

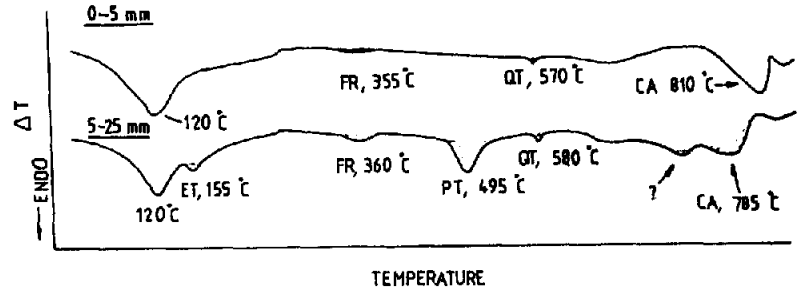

FIG. 5.
DTA thermograms for slab 3. (Key: ET: Ettringite, FR: Friedel's salt, PT: Portlandite, QT: α-Quartz, CA: Calcite).

Although the XRD results indicates the presence of ettringite at both the above depth intervals, the DTA thermograms confirm its presence for the 5–25 mm depth interval alone with a well defined endothermic peak centered at 155°C. This is despite the XRD diffractograms for both the depth intervals show the maximum intensity peaks of almost identical intensities. Thus, the well defined peak in the XRD diffractogram for the 0–5 mm depth interval which was believed to be the ettringite might be due to the presence of another phase having a d-spacing similar to the ettringite.

Slab 10. Figure 6 depicts the XRD diffractograms for 0–5 mm and 5–25 mm depth intervals. This particular slab was cast with 65% cement replacement with GGBFS. The results from the

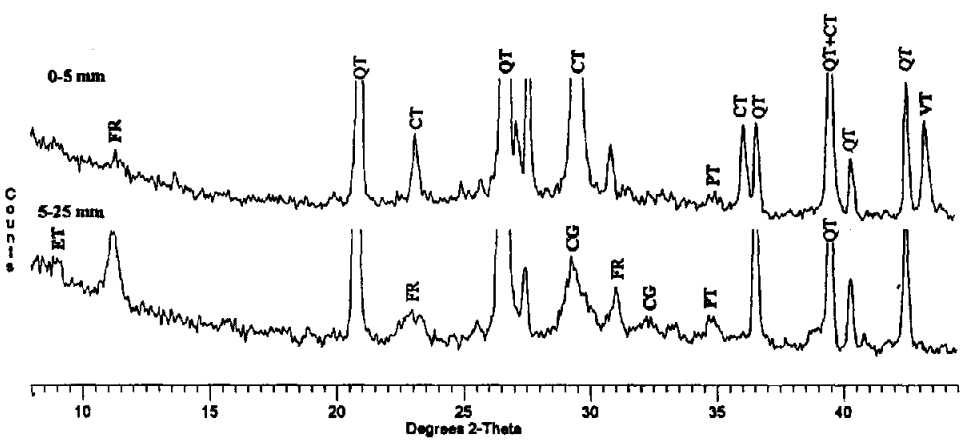

FIG. 6.
XRD diffractograms for slab 10. (Key: ET: Ettringite, FR: Friedel's salt, PT: Portlandite, QT: α-Quartz, AT: Aragonite, CT: Calcite, CG: C-S-H gel and VT: Vaterite. The keys in bold letters indicate the 100% intensity peaks).

0–5 mm and 5–25 mm depth intervals emphasise the observations already made for slab 3. The diffractogram for the 0–5 mm depth interval shows almost diminishing maximum intensity peaks for the Friedel's salt and portlandite in the presence of dominant peaks for calcite and vaterite. The diminution in the quantity of portlandite is due to the combined action of atmospheric carbonation and the pozzolonic reaction by the GGBFS. According to the diffractogram ettringite is not present.

On the other hand, the XRD diffractogram for the 5–25 mm depth interval shows a comparatively clear and fairly big maximum intensity peak for the Friedel's salt in the absence of a maximum intensity peaks for calcite and vaterite. The typical broad peak present in the region of the maximum intensity peak for calcite indicates the presence of poorly crystalline C-S-H gel. A small maximum intensity peak for portlandite is also evident, although a fairly big peak was expected due to the total absence of carbonation. This, however, might be due to the dominant pozzolonic reaction by the GGBFS at this depth interval. The diffractogram also indicates the presence of ettringite in trace amounts.

Figure 7 presents the DTA thermograms for 0–5 mm and 5–25 mm depth intervals. The thermogram for the 0–5 mm depth interval, contrary to the XRD results indicate the absence of both Friedel's salt and portlandite. This, however, is believed to be due to their insignificant presence as already seen from XRD; the related thermal events might be below the sensitivity of the particular DTA. Alternatively, in conformity with the XRD observation the thermogram indicates the presence of ettringite. A dominant endothermic peak centered at 795°C indicates the presence of calcite, which confirms the XRD results.

On the other hand, in accordance with XRD results, the thermogram for the 5–25 mm depth interval shows a well defined dominant endothermic peaks centered at 355°C and 155°C to indicate the presence of Friedel's salt and ettringite respectively. No endothermic peak is seen around 800°C, which implies that the typical broad peak observed on XRD diffractogram in the vicinity of the maximum intensity peak for calcite is definitely due to the poorly crystalline C-S-H gel. The portlandite present in trace amounts as already observed from XRD is not seen on the DTA thermogram. The reason for this is already explained above for the 0–5 mm depth interval.

Thus, both the slabs 3 and 10 at 0–5 mm depth interval showed a diminution in the quantity of Friedel's salt in the presence of strong atmospheric carbonation. However, the amount of Friedel's salt increased at greater depths where atmospheric carbonation was not dominant.

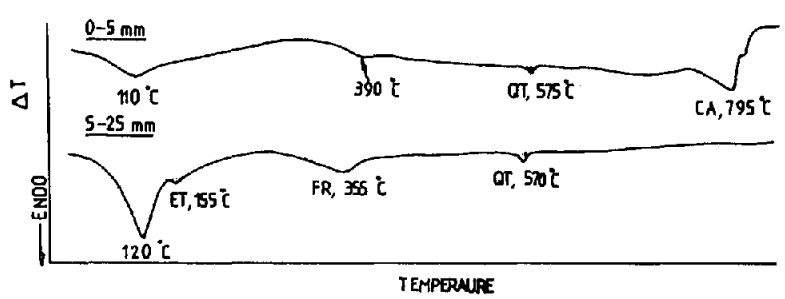

FIG. 7.

DTA thermograms for slab 10. (Key: ET: Ettringite, FR: Friedel's salt, PT: Portlandite, QT: α-Quartz, CA: Calcite).

Although etrringite was not present at 0–5 mm depth interval its presence similar to that of Friedel's salt was noticeable at greater depths.

Slab 1. Figures 8 and 9 illustrate the XRD diffractogram and the DTA thermogram respectively for 0–5 mm depth interval. The XRD diffractogram indicates the co-existence of the phases such as calcite, aragonite, vaterite, Friedel's salt, portlandite and ettringite with clearly defined peaks.

The DTA thermogram confirms the findings of XRD. Well defined endothermic peaks centered at 795°C and 490°C indicate the presence of calcite and portlandite respectively. On the other hand, the relatively indistinct endothermic peaks centered at 330°C and 155°C show the presence of Friedel's salt and ettringite respectively. This was the only slab out of the four slabs examined so far, in which for the 0–5 mm depth interval a well defined endothermic peak for portlandite is present. The above evidence strongly suggests the lowest degree of carbonation at the 0–5 mm depth interval for slab 1, and this is quite understandable because of its low w/b ratio of 0.45.

Discussion

In the present investigation, as already explained before, the slabs were exposed to a total of 70 exposure cycles in four steps, with smaller (few days) time gaps between 10 and 20, 20 and 50 steps of cycles and a longer time gap (about one and half year) between the 50 and 70 cycles. Each exposure cycle consisted of 7 days of ponding followed by 3 days of drying. After completing such 70 cycles the slabs were exposed to internal laboratory environment for about two and half years. Carbonation is not expected during the wetting periods as the air permeability of concrete decreases markedly above 80% RH (22); however, at 50% RH the carbonation is at its maximum rate (14). The RH controls the diffusion rate of atmospheric CO_2 through the concrete, the diffusion rate decreases with increasing RH. A minimum moisture requirement is essential to dissolve the CO_2 to form carbonic acid, which in tern reacts with the portlandite. During the drying cycle, the capillary pores become emptied and this facilitates an

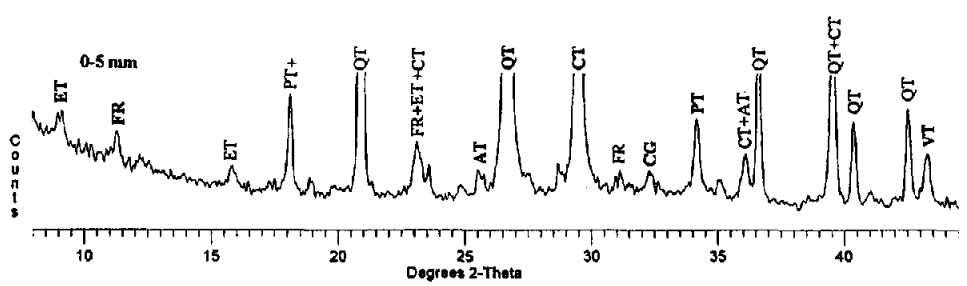

FIG. 8.
XRD diffractogram for slab 1. (Key: ET: Ettringite, FR: Friedel's salt, PT: Portlandite, QT: α-Quartz, AT: Aragonite, CT: Calcite, CG: C-S-H gel and VT: Vaterite. The keys in bold letters indicate the 100% intensity peaks).

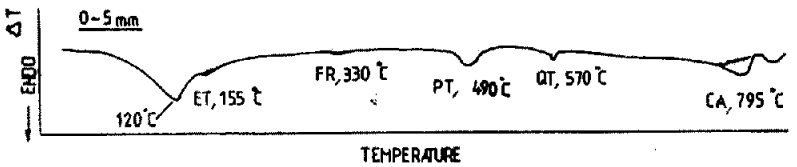

FIG. 9.
DTA thermogram for slab 1.(Key: ET: Ettringite, FR: Friedel's salt, PT: Portlandite, QT: α-Quartz, CA: Calcite).

enhanced diffusion rate for the CO_2 through the concrete cover. Hence, the concrete may start carbonating during the drying process at some rate, although may not be at an optimum rate continuously. However, the net drop in pH due to the carbonation occurring during a 3 days drying period of the 10 days cycle might be negligible due to the re-alkalisation (due to cement hydration), that might take place during the 7 days ponding as soon as the next 10 days cycle begins.

The scenario will change once the slabs complete the first step (10 cycles) of exposure cycles to 4% NaCl solution. This is because, the chloride ions diffused through the concrete after the first step of cycles will assist in the carbonation process during the time gap before the commencement of the next step of exposure cycles. This is explained by the moisture retention ability of the chloride ions, thus, retarding the drying process during the time gaps between the steps of cycles. However, in the present case, the significant amount of carbonation is believed to have taken place during the one and half years time gap between the 50 and 70 cycles and also during the two and half years time gap after the completion of 70 cycles. Thus, the significant atmospheric carbonation has taken place in the drying laboratory environment similar to that of an interior of a building.

From the DTA thermograms presented in Figures 3, 5, 7, and 9 it is clear that, of all the four slabs considered, slab 11 (w/b = 0.6) was severely carbonated at 0–5 mm depth interval. This slab (11) showed the biggest endothermic peak, on the other hand, slab 1 showed the smallest endothermic peak centered around 800°C to indicate the presence of calcite. By taking height of the endothermic peak as a criterion, the degree of carbonation, in decreasing order, is given by slab 11 (w/b = 0.6), slab 3 (w/b = 0.75), slab 10 (w/b = 0.75, with slag) and slab 1 (w/b = 0.45). Investigations are underway to know the cause for the differences in the carbonation rates, although for slabs 1 and 3 the role of w/b ratio is apparent.

It is also evident from the Figures 3, 5, 7 and 9 that, for the 0–5 mm depth interval, the biggest endothermic peak for portlandite happens to be for the slab 1. Slab 3 did not show the endothermic response for the portlandite on DTA, however, its presence was observed in trace amounts on XRD diffractograms, while slab 11 did not show the presence of portlandite on both DTA and XRD. Thus, a comparison based on the extent of the presence of portlandite also tells the degree of carbonation in the slabs to occur in decreasing order, in slab 11, and slab 3, and slab 1. However, this criterion for slab 10 (with slag) might lead to an error due to the additional pozzolonic reaction by the GGBFS.

For slab 11 at 0–5 mm depth interval both Friedel's salt and portlandite were absent and it was severely carbonated at the above depth interval. For slabs 3 and 10, both Friedel's salt and portlandite were present in trace amounts, and these slabs were carbonated to a relatively lesser

extent than slab 11. However, slab 1, the least carbonated of all the four showed the co-existence of Friedel's salt and portlandite in appreciable quantities with calcite and vaterite. The slabs 3, 10 and 11 consistently showed the presence of Friedel's salt at greater depths where the concrete was not carbonated, except for slab 3 in which a relatively lower degree of carbonation was evident at 5–25 mm depth both from DTA and XRD. These results obviously suggest the stability of the Friedel's salt to be dependent on the alkalinity of the concrete surrounding it. The solubility of Friedel's salt increases with the degree of carbonation of the concrete. The solubility of the Friedel's salt is in accordance with the equilibrium given below. Note that, $Al(OH)^-_4$, is an aluminium containing ion known to exist in concrete (23).

$$3CaO.Al_2O_3.3CaCl_2.10H_2O \leftrightarrow 4Ca^{2+} + 2Cl^- + 4OH^- + 2Al(OH)_3 \quad (1)$$

$$Al(OH)_3 + OH^- \leftrightarrow Al(OH)^-_4 \quad (2)$$

From the above solubility equilibrium for the Friedel's salt it is clear that, in the event of a drop in alkalinity due to carbonation, the chlorides from the Friedel's salt are released into the pore solution. Thus, in the presence of carbonation attack the steel reinforcement in chloride contaminated concrete structure is at a higher corrosion risk. This may also explain the corrosion risk presented by the presence of chlorides at low concentrations, which is generally negligible in uncarbonated concrete, but became increasingly significant on carbonation (24).

The DTA thermograms for the slabs 11, 3 and 10 confirmed the absence of ettringite at 0–5 mm depth interval while, its presence was confirmed at greater depths where there was no carbonation (lower degree of carbonation for slab 3). This suggests that, the stability of ettringite is also pH dependant as reported in literature (23,25). Ettringite is known to be unstable below a pH around 10.5 to 10.7 and dissolves as gypsum and aluminium sulphate (25). This evidence indirectly suggests that, the pH at 0–5 mm depth interval for slabs 11, 10 and 3 was definitely below (less alkaline) 10.5 to 10.7 pH range, while for slab 1 the pH was higher (more alkaline) than the above pH range.

Conclusions

The following conclusions are drawn from the present investigation.

1. The stability of Friedel's salt in chloride contaminated concrete is pH dependant. The solubility of Friedel's salt increases with the degree of atmospheric carbonation of concrete.
2. Ettringite does not exist in severely carbonated concrete as its stability is also pH dependant.
3. To confirm the phases present in hydrated cements the results from XRD alone are inadequate. Results from thermal studies such as DTA are essential to support the XRD results.
4. Severe carbonation of chloride contaminated structural concrete is also possible in indoor drying laboratory environment similar to that of an interior of a building.
5. Peak heights due to calcite and portlandite from the DTA thermogram can be used as a criterion to estimate the degree of carbonation occurring in concrete structural elements. However, in the presence of mineral admixtures, an estimation based on the presence of portlandite leads to an error due to the pozzolonic reaction.

Acknowledgements

The authors would like to thank DR. R.A. Buckly and Prof. J.H. Sharp of the Department of Engineering Materials, University of Sheffield, for their assistance during the XRD and DTA studies respectively.

References

1. F.E. Jones, Proc. 4th International Symposium on Chemistry of Cements, NBS Monograph 43, Washington, 205(1962).
2. S. Chatterjee, Cem. Concr. Res.8, 461(1978).
3. V.S. Ramachandran, R.C. Seeley and G.M. Poolmark, Materials and Constructions, 17, 285(1984).
4. V.S. Ramachandran, Materials and Constructions, 4, 143(1971).
5. S. Diamond, Cement Concrete and Aggregates, 8, 97(1986).
6. J.J. Beaudoin, V.S. Ramachandran and R.F. Feldman, Cem. Concr. Res. 20, 875(1990).
7. P. Lambert, C.L. Page and N.R. Short, Cem. Concr. Res. 15, 675(1985).
8. C.L. Page, N.R. Short and A. El Tarras, Cem. Concr. Res. 11, 395(1981).
9. S. Ehtesham Hussain, Rasheeduzzafar and A.S. Al-Gahtani, Cem. Concr. Res. 21, 8(1994).
10. Rasheeduzzafar, ACI Materials Journal, 89, 574(1992).
11. A.K. Suryavanshi, J.D. Scantlebury and S.B. Lyon, Cem. Concr. Res. 25, 581(1995).
12. Taylor Woodrow Research Laboratory, Concrete in the Oceans Project, Technical Report No-5, Part II, 76(1980).
13. C.L. Page and O. Vennesland, Materials and Constructions, 16, 19(1983).
14. O.E. Gjorv, Proc. of EVALMAT, 565(1989).
15. BS 1881: Part 124, Determination of Chloride Contents, 17(1988).
16. Highway Research Board, Guide to Compounds of Interest in Cement and Concrete Research, Highway Research Board Special Report No.127, 28(1972).
17. V.S. Ramachandran, Calcium Chloride in Concrete, p.107, Applied Science Publisher, London, 1976.
18. H.F.W. Taylor, Cement Chemistry, p.177, Academic Press, London, 1990.
19. V. Kasselouri, G. Dimopoulos and G. Parissakis, Cem. Concr. Res. 25, 477(1995).
20. H.E. Schwiete and U. Ludwig, Proc. 5th International Symposium on the Chemistry of Cements, Tokyo, Part II, 37(1968).
21. V. Pavlik, Cem. Concr. Res. 24, 1495(1994).
22. R.K. Dhir, P.C. Hewlett and Y.N. Chan, Magazine of Concrete Research, 41, 137(1981).
23. D. Damidot and F.P. Glasser, Cem. Concr. Res. 23, 221(1993).
24. K. Muller, Proc. RILEM International Symposium, Budapest, 9(1986).
25. A. Gabrisova, J. Havlica and S. Sahu, Cem. Concr. Res. 21, 1023(1991).